Journal of Glaciology

Paper

Cite this article: Hannula H-R, Pulliainen J (2019). Spectral reflectance behavior of different boreal snow types. *Journal of Glaciology* **65**(254), 926–939. https://doi.org/10.1017/jog.2019.68

Received: 31 May 2018
Revised: 12 August 2019
Accepted: 13 August 2019
First published online: 30 September 2019

Key words:
Remote sensing; snow; snow microstructure

Author for correspondence:
Henna-Reetta Hannula, E-mail: henna-reetta.hannula@fmi.fi

cambridge.org/jog

Spectral reflectance behavior of different boreal snow types

Henna-Reetta Hannula and Jouni Pulliainen

Space and Earth Observation Centre, Finnish Meteorological Institute, PL 503, 00101 Helsinki, Finland

Abstract

Spectral reflectance of natural snow samples representing various stratigraphies was investigated in a controlled dark laboratory environment. Mean and Std dev. of band specific reflectance values were determined for several satellite sensor bands utilized in remote sensing of snow. The reflectance values for dry, moist, wet and wet and littered snow for different instruments varied between 0.63–0.97 in the visible and near-infrared bands at an incoming light zenith angle of $\theta = 55°$. The results indicate that in MODIS band 4 (545–565 nm), essential to snow mapping, the reflectance of snow drops by 9% when dry snow changes to wet snow and by a further 10% when typical forest litter inclusions exist on the wet snow surface. A separate investigation of individual snow types revealed that they can be grouped either as dry or wet snow based on their spectral behavior. However, some snow types were located between these two distinct groups, such as snow with near-surface melt-freeze crusts, and could not be clearly distinguished. The reflectance statistics collected and analyzed here can be directly used to refine accuracy characterization and parametrization of snow mapping algorithms, such as the SCAmod method, used for the mapping of snow cover area.

1. Introduction

Seasonal snow cover is linked with the surrounding environment through feedback mechanisms which may intensify or weaken global environmental change. Because snow has high surface albedo, the extent of terrestrial snow cover has a significant effect on the planetary radiation budget (Groisman and others, 1994; Brown and Robinson, 2011). The disappearance of snow or changes in the snow depth or in the length of the snow cover period will induce changes in the underlying permafrost, seasonal soil frost and in the vegetation carbon uptake further linking the snow cover changes with the global carbon cycle (Pulliainen and others, 2017). These make the extent and duration of snow cover vital variables for climate change research (Vaughan and others, 2013) and emphasize the need for continuous and correct snow cover information.

Due to the high reflectance of snow in the visible (VIS) and near infrared (NIR) parts of the electromagnetic spectrum, optical satellite remote sensing is an efficient method to monitor the extent and duration of snow cover (Dietz and others, 2012). By nature the snow reflectance is variable both spatially and temporally, and it exhibits considerable changes, from the dry snow period through the melt season due to snow metamorphism, melting, addition of impurities and changing measurement and illumination geometry (Warren, 1982; Hall and others, 1992; Winther, 1993; Pulliainen and others, 2014). The dependency of different snow reflectance quantities on the prevailing environmental and observational conditions, and their implications for optical remote sensing have been widely investigated in the literature (Zhou and others, 2003; Dozier and others, 2009; Painter and others, 2009). Spectral unmixing or inverse model-based methods can be used to retrieve the snow cover area (SCA), or within a satellite pixel, the fractional snow coverage (FSC) from the optical satellite data (Vikhamar and Solberg, 2002, 2003; Painter and others, 2003, 2009; Metsämäki and others, 2005, 2012, 2015; Dozier and others, 2009). These methods describe the scene reflectance as a combination of spectral signatures of model parameters (i.e. end-members), such as snow, forest canopy and snow-free ground. Thus the derived snow cover estimates are sensitive to the inadequate description of the predetermined input parameter variability, such as snow reflectance that is further propagated to the uncertainty of the snow cover maps (Salminen and others, 2009, 2018; Metsämäki and others, 2015). The reflectance of an end-member and its variability can be determined by field measurements, modelling or by the optical satellite data itself. The variability of the snow reflectance, on the other hand, is a function of its physical properties such as liquid water content and grain size but is also dependent on the view-illumination geometry (Vikhamar and Solberg, 2002). Thus snow reflectance information gathered in the laboratory or in the field with concurrent in situ measurements, describing the micro- and macro-physical characteristics of snow, can be utilized to further develop the snow algorithms used in satellite remote sensing, and to decrease the existing uncertainties of retrievals.

In this study, earlier estimates of snow reflectance obtained by modelling (Green and others, 2002; Painter and Dozier, 2004; Kokhanovsky and others, 2005) and field measurements (Aoki and others, 2000; Peltoniemi and others, 2005; Salminen and others, 2009) were complemented and extended by quantifying snow reflectance variability under controlled laboratory conditions by measuring a notable amount of undisturbed samples of natural boreal

snow. The aim was to investigate the effects of snowpack characteristics, including organic matter inclusions, without the typical inaccuracies related to field measurements (due to changes in illumination conditions between measurements, tilts in snow surface/surface roughness and challenges in calibration), and thereby, offer more accurate snow reflectance information to be used as an input for snow cover mapping algorithms.

The four main snow types investigated were (1) dry snow; (2) moist snow; (3) wet snow and (4) wet snow with a littered snow surface. Six different dry snowpack conditions were investigated and one snow occasion represented dry snowpack with moist surface snow. Spectroradiometer observations from wet snow samples with an un-littered surface were obtained for two occasions and one measurement occasion represented wet snow with a littered surface. Multiple samples for each snow condition were measured and Std dev. for each snow type was defined from sample-wise reflectance variability. Although the most important impurities decreasing snow surface albedo are soot, continental dust and volcanic ash (Warren, 1984), the organic material originating from surrounding trees and snow-free patches (Winther and others, 1999) lower the snow surface albedo and enhance the solar absorption. This increases snowmelt and changes snow surface roughness when the litter particles are melting through the snow and may hamper SCA estimation from satellite data (Melloh and others, 2001). However, there has been little investigation regarding the effect of the organic material on snow spectral reflectance, although this may be a significant factor during the melt season, in particular in forested areas.

The measurement data of different snow types were resampled to correspond to various relevant satellite instrument bands with slightly different band configurations, in order to quantify the effect of these differences on the snow reflectance. This comparison indicates the possible effect of slightly varying channel configurations on snow reflectance, which is relevant concerning the use of different satellite instruments (e.g. Sentinel-2 and −3) for the mapping of snow cover. These algorithms typically apply reference (end-member) reflectances of the Earth's surface spectral contributors (Vikhamar and Solberg, 2002, 2003; Painter and others, 2003, 2009). In addition, resampling of reflectance of all the measured snow types to correspond to various bands of one sensor, moderate-resolution imaging spectroradiometer (MODIS), was implemented, and the corresponding normalized difference snow index (NDSI) calculated to investigate the sensitivity of these often applied band indices for varying snow microstructures. Finally, the results obtained here were compared with the field dataset (Salminen and others, 2009) currently used for the characterization of the snow reflectance and its variability in the semi-empirical reflectance model-based method (SCAmod), operated by the Finnish Environment Institute (SYKE) (Metsämäki and others, 2005, 2012, 2015). The SCAmod method derives the fractional snow coverage within a satellite pixel by inverting a radiative transfer-based forward model which describes the scene reflectance as a combination of snow-free ground, (wet) snow cover and forest canopy. An average and Std dev. of snow reflectance has been determined from observations executed in various illumination and snow circumstances. Thus the measured reflectance variability is due to both changes in illumination conditions and in the snow properties which may result in increased uncertainty in the FSC estimate.

2. Quantification of snow reflectance variability

In earlier research, the effects of the snow microstructure on the reflective properties of snow, and *vice versa*, the retrieval of different quantitative snow parameters (e.g. surface albedo and grain size) from snow reflectance data have been studied through models (Xie and others, 2006; Painter and others, 2009). The characteristics of snow reflectance have been studied both in the field, and in the laboratory with artificial snow or by destroying the original snow microstructure (Nakamura and others, 2001; Kaasalainen and others, 2006). To our knowledge, only Dumont and others (2010) have executed bidirectional reflectance distribution function (BRDF) laboratory measurements with four ($n = 4$) natural undisturbed (alpine) snow samples. In the initial state three of these samples represented wet snow and one dry snow. Although controlled laboratory measurements (Zender and others, 2009; Hadley and Kirchstetter, 2012; Lv and Sun, 2014) may offer valuable information, these may not capture the complexity of snow under natural conditions. The advantages in the laboratory, however, are the control of exact geometrical measurement conditions and the almost nonexistent part of the diffuse irradiation (Sandmeier and others, 1998). The disadvantages are the possible mechanical and thermal stress that may affect the microstructure of the snow sample during sampling and between the time of the sampling and the measurements, the difference between the lamp and the sun irradiance with respect to remote sensing applications, and the possible fluctuations of the artificial illumination intensity. Available facilities, size of the sampled snow and the characteristics of the sample container often limit the measurement geometries in the laboratory. On the other hand, it is difficult to control all the desired parameters in the field. In particular, the portions of diffuse and direct components of light, which are dependent on cloud cover and atmospheric composition, affect irradiation spectral distribution (Warren, 1982) and can change fast.

The measured reflectance values of this study approximate to the conical–conical reflectance factor (CCRF), the measureable quantity of the bidirectional reflectance factor (BRF) (Schaepman-Strub and others, 2006). BRF is defined as the ratio of the reflected radiant flux of a distinct surface area to the reflected radiant flux of a perfectly Lambertian surface of the same area in the same view and illumination geometry (Nicodemus and others, 1977). Here, the general term of *spectral reflectance* is used to refer to CCRF. Field and satellite sensor reflectance measurements are usually mentioned to approximate to BRF if the illumination is composed only of a direct component and the field of view (FOV) is small (Bruegge and others, 2000). Top-of-atmosphere reflectance observed by a satellite can be converted to a bottom-of-atmosphere (BOA) value by using an atmospheric correction which is also a significant source of error in the BOA estimates (Claverie and others, 2018). As such, laboratory results can be compared with reflectance values observed in the field and from a satellite under clear sky conditions. However, the instrument FOV and the angular pattern of the incoming irradiance are always different between the measurements made from a satellite and those executed at ground or in a laboratory (even if atmospheric correction is assumed to be ideal).

3. Material and methods

3.1. Snow sample collection and reference data

All measurements were made in the Arctic Space Centre of the Finnish Meteorological Institute (FMI-ARC), located in Sodankylä, northern Finland (67.368 N, 26.633 E). The measurements were conducted over eight days in the springs of 2013–15 and were executed in a dark laboratory. Snow samples were collected in the immediate vicinity of the laboratory – with one exception in 2014 when samples were collected from a nearby wetland site.

For each snow type, several samples (sampled from the same ~ 5 m × 5 m homogeneous area) were taken and measured. The snow was sampled by cutting an even wall into the snowpack

https://doi.org/10.1017/jog.2019.68 Published online by Cambridge University Press

and carefully pushing an aluminium sampler (35 cm × 35 cm) into the snow, placing the sample in an insulated black box after removal. The measurement room had been cooled by air conditioning and cool air flowing from outside while moving the samples, but air temperatures below zero were not achieved. The snow sampler had been painted inside with a black matte color and the sampler depth was 23 cm. The maximum penetration of light into snow occurs around the blue region (Warren, 1982). King and Simpson (2001) reported 480 nm irradiance to decrease into ~3% of the original value at the depth of 20.5 cm within homogeneous snow with a typical grain size of 0.2 mm and a density of 0.24 g cm^{-3}. Comparison of several measurement results of liquid equivalent e-folding depths (density scaled penetration depth) for snow presented by King and Simpson (2001) showed a maximum penetration depth of 6.5 cm. As such, we considered the sample to be deep enough to minimize the absorbing effect from the sampler bottom.

All sampling dates, snow types and the corresponding acronyms are presented in Table 1. During the first measurement day, dry snow from a shadowed area (D_shadow13) and an area exposed to direct sunlight (D_sun13) were sampled. During the second laboratory day, samples from pure wet snow (W_pure13) and wet snow affected by surface litter (W_litter13) were collected. The litter was mainly composed of yellowish needles and seeds fallen from the nearby pine and birch trees, and in part of the cases, of brown-yellow thin fragments of bark and grey lichen. In 2014–15, four dry snow types, D_decomposed14, D_crust14, D_dendrites15 and D_small15, one dry snow type with moist surface snow M_rimed14, and one wet snow type W_pure14 were sampled. The acronyms follow the sampling year and the snow type in general (wet/moist/dry/pure/litter) or is referring to the snow grain type on the sample surface. The snow type was defined wet if the average fraction of liquid water was ≥ 3% (Fierz and others, 2009) and the snow temperature profile was at 0 C° indicating melting. Accordingly, the snow type was considered dry if the fraction of liquid water was <1% and the snow temperature profile was below 0 C°. The temperature profile of M_rimed14 was otherwise below zero but the moist surface layer was affected by the above zero air temperatures. Thus we separated M_rimed14 as moist snow. An example of the snow sample of D_sun13, W_pure13 and W_litter13 is presented in Figure 1.

Snow pit measurements were made at representative sites of each sampling area in order to record the differences between the snow types. Snow layers were visually detected based on hardness, density and grain size differences. Snow grains of each layer were macro-photographed against a one millimetre grid, and the average snow grain size was discretized to every 0.25 mm on the basis of the typical maximum grain diameter (D_{max}). A snow grain type for each layer was defined (Fierz and others, 2009). The specific surface area (SSA) of the snow grains in every 3 cm was measured with IceCube, manufactured by A2 photonic sensors, France (Gallet and others, 2009). The instrument measures hemispherical reflectance of snow at 1310 nm which is related to SSA (e.g. Domine and others, 2006). The SSA-value describes the relationship of the snow grain surface area to its volume. An optically equivalent ice sphere diameter of the snow grains (D_0) can be derived from the SSA values by using the theoretical relationship between SSA and the optical grain diameter (e.g. Kokhanovsky and Zege, 2004). However, IceCube was not available during all the measurement days and on 18 April 2013 the snowpack was very wet, possibly too wet for laser detection, the measurement principle of the instrument. Thus these results should be interpreted with care. Additionally, temperature (every 10 cm) and density (every 5 cm) profiles were recorded, and Snow Fork (Sihvola and Tiuri, 1986) measurements, offering density and liquid water content information, were made every

Table 1. The sampling dates (YYYYMMDD), the snow types measured and the corresponding snow type acronyms during the laboratory experiments

Sampling date	Snow type	Acronym	Air (° C)	Snow fork wetness (%)	Snow cutter density (kg m^{-3})	*Ave. D_{max} (mm) 23 cm*	Ave. D_0 (mm) 23 cm	Ave. D_{max} (mm) 10 cm	Ave. D_0 (mm) 10 cm	No. of snow samples	ASD Number of spectra per snow sample
20150323	Dry	D_small15	−3.9	0.71	231	*0.57*		0.40		15	10
20150202	Dry	D_dendrites15	−12.7	-	148	*0.57*	0.20	1.00	0.17	15	10
20130321	Dry	D_sun13	−6.2	-	232	*0.63*	0.37	0.50	0.33	15	30
20140227	Dry	D_crust14	−1.3	0.76	232	*0.63*		0.50		15	20
20140220	Dry	D_decomposed14	−9.9	0.84	192	*0.66*	0.32	0.55	0.26	12	20
20140327	Moist surface	M_rimed14	3.2	0.91	271	*0.73*		0.50		12	20
20130321	Dry	D_shadow13	−6.2	-	220	*0.75*	0.38	0.75	0.35	9	30
20130418	Litter	W_litter13	2.9	7.57	373	*1.00*	2.33**	1.00	2.21**	25	30
20140416	Wet	W_pure14	3.4	2.97	367	*1.05*	1.34	1.00	1.44	15	20
20130418	Wet	W_pure13	2.3	5.31	387	*1.33*	2.45**	1.00	2.39**	25	30

Air temperature during each sampling date, the average liquid water content and the average density for the sampled snow depth of 23 cm are presented. The typical visual maximum grain diameter (D_{max}) was weighted by the respective layer depth and averaged separately for the whole snow sample depth and for the 10 cm surface layer. The optical equivalent grain diameters (D_0), derived from the averaged SSA-values, are accordingly presented if measurement data were available. SSA measurements in 20130418 are marked with **as the snow wetness might have been in the limit of the measurement capability of the instrument. In the last two columns, the number of snow samples taken from each snow type and the number of spectral acquisitions executed from each snow sample are shown. Snow types are ordered by increasing average D_{max} (23 cm).

https://doi.org/10.1017/jog.2019.68 Published online by Cambridge University Press

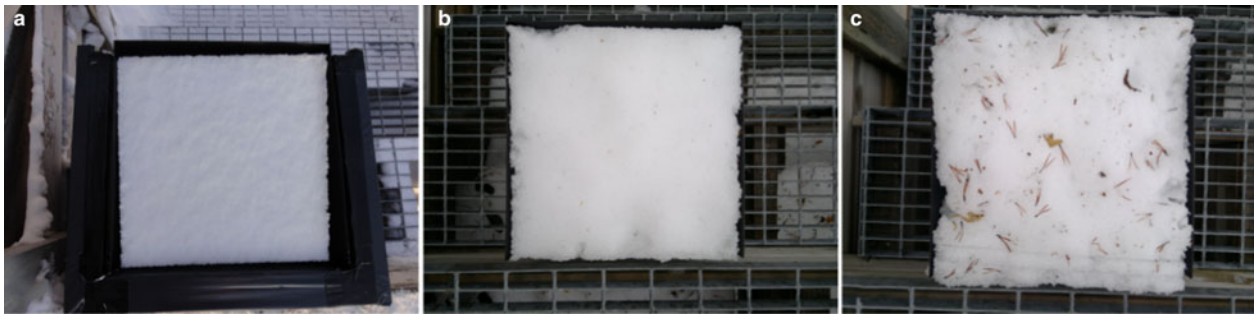

Fig. 1. Example of (a) a dry snow sample ($D_{\_sun13}$), (b) a wet and pure snow sample ($W_{\_pure13}$) and (c) a wet and littered snow sample ($W_{\_litter13}$).

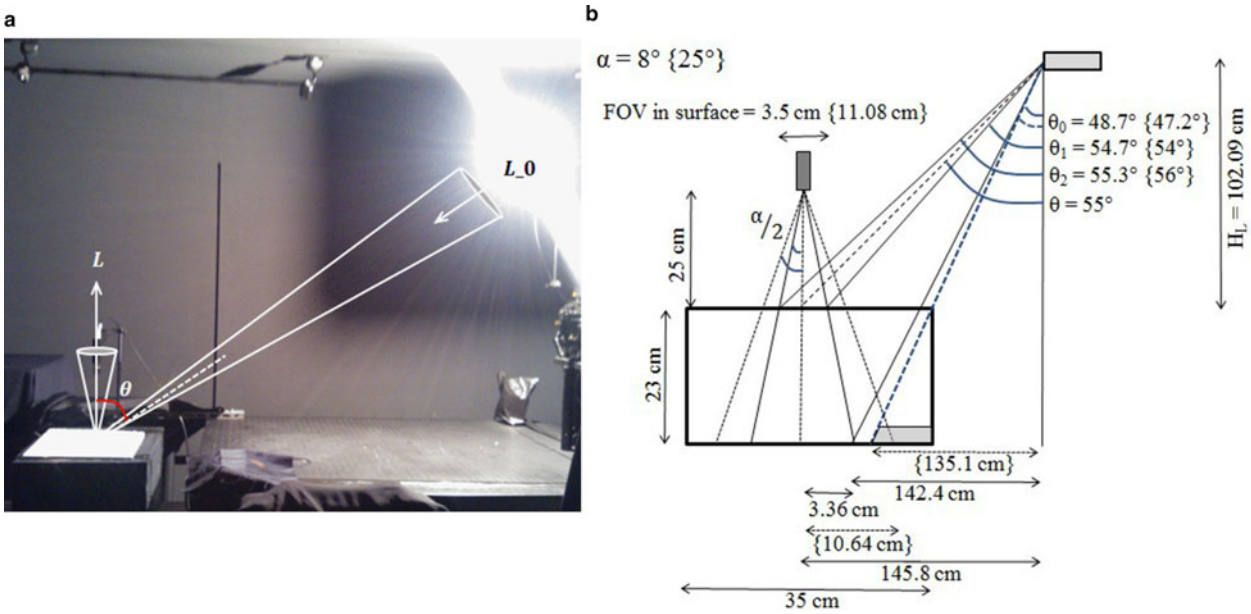

Fig. 2. A photo and a schematic of the laboratory measurement setup. (a) The measured reflectance values were defined to approximate to the CCRF, the measurable quantity of the BRF (Schaepman-Strub and others, 2006) and analogously to Salminen and others (2009). The light zenith angle during the measurement is denoted by θ. In (b) the geometric details of the measurements are shown including the effect of the non-collimated light source on the actual incident zenith angles/irradiance levels. The transparent grey box in the sample bottom illustrates the area (not in scale) shaded by the sample holder edge when the 25° FOV was used. The angle θ_0 for 25° FOV is represented with a dashed line.

10 cm. Every snow sample of $W_{\_litter13}$ was photographed for later analysis of the surface organic matter contents.

3.2. Laboratory setup

The collected snow samples were measured with an ASD Field Spec Pro JR Spectroradiometer (ASD Inc., Boulder, Co, USA). The instrument measures spectral radiance between 350–2500 nm with one silicon photodiode array (350–1050 nm), and two indium gallium arsenide photo-diode detectors (900–1850 nm and 1700–2500 nm). The measurement head was set at nadir at a height of 25 cm from the snow sample surface (Fig. 2). In 2013 a bare fiber optic with FOV of 25° was used. In 2014–15 a foreoptic with FOV of eight degrees was used. These corresponded to footprint sizes (support) of 3.5 cm and 11.08 cm for 8° and 25° FOV, respectively. The small footprint reduced the effects of nonparallelism of the light source (Sandmeier and others, 1998), which was a 1000 W Tungsten halogen lamp, calibrated to 250–2500 nm. During measurements, the lamp current was controlled and kept at 8 (± 0.0008) A.

One light zenith angle ($\theta = 55°$) was used resembling the typical sun zenith angle at high latitudes during late spring. To solve the spectral reflectance, a calibrated white reference panel (Spectralon) representing a nearly Lambertian reflector was measured at the beginning and at the end of each measurement session. From each snow sample, 10–30 spectra were measured at one second intervals (Table 1). The number of individual spectral acquisitions was decreased from 30 and 20 to 10 when snow types representing new or nearly new snow were to be measured as these snow types are subject to fast metamorphism.

3.3. Spectral data post-processing

In post-processing the (30/20/10) spectra of each snow sample were averaged. The average absolute reflectance $R(\lambda, \theta)$ of the snow was determined at each wavelength:

$$R(\lambda, \theta) = R_{\mathrm{Cal}}(\lambda) \times \frac{L(\lambda, \theta)}{L_0(\lambda, \theta)} \quad (1)$$

where $R_{\mathrm{Cal}}(\lambda)$ is the spectral calibration coefficient of the white reference panel provided by the manufacturer, $L(\lambda, \theta)$ is the averaged radiance (W m^{-2} sr^{-1} nm^{-1}) of snow at the wavelength λ and at the light zenith angle θ and $L_0(\lambda, \theta)$ is the measured average radiance of the reference panel. An average and Std dev. of spectral reflectance for each snow type were determined based on spectral data of the snow samples, i.e. Std dev. indicates the deviation between different snow samples of each investigated snow type.

https://doi.org/10.1017/jog.2019.68 Published online by Cambridge University Press

To assess the implications of different snow types and various band configurations for SCA estimation, spectrometer-derived spectral reflectances were resampled to correspond to relevant instrument channels specified in Table 2. For each snow sample measurement, a weighted average based on the wavelength dependent relative spectral response functions (SRF) made available by the data providers was calculated. The snow samples were grouped as dry snow (all dry snow types), moist snow ($M_{\_rimed14}$), wet snow ($W_{\_pure13}$ and $W_{\_pure14}$), or wet and littered snow ($W_{\_litter13}$) and an average and Std dev. (deviation between different samples of the same snow type) of the observed reflectance at each band was determined. To investigate the sensitivity of band reflectance on varying snow microstructures, separate resampling of all the measured snow types to correspond to bands of one sensor, MODIS, was implemented, and the respective NDSI indices calculated. MODIS is currently one of the most widely used instruments for SCA mapping. The amount of the organic material for $W_{\_litter13}$ was determined from digital images by comparing the number of pixels consisting of organic litter vis-à-vis to pixels consisting of pure snow within the FOV of the instrument.

Finally, average and Std dev. of MODIS band specific reflectances for wet and dry snow types were compared with those obtained by field spectroscopy and provided by Salminen and others (2009). Reflectance characterization of the SCAmod method currently relies on this field dataset. The field measurements have been collected in the surroundings of FMI-ARC in 2007–08 with a similar ASD Field Spec instrument as used in this study and the average and Std dev. of reflectance for wet and dry snow represent conditions described in Table 3. Snow was categorized as wet or dry based on snow temperature measurements and the so-called snowball test. If the snowpack surface was moist the snow type was categorized as wet.

3.4. Geometric limitations and sources of error and uncertainty

With a noncollimated light source, the irradiance reaching different points of the snow sample had a gradient. Figure 2b shows how the light zenith angles corresponding to the irradiance reaching the nearest (θ_1) and furthest (θ_2) points of the nominal FOV on the sample surface, as well as the angle corresponding to the irradiance reaching the FOV edge in the snow sample bottom (θ_0) are deviated from $\theta = 55°$, determined for the middle point below the measurement head. The responsivity of the ASD optic fibers is not uniform within the FOV meaning that radiance at different wavelengths may have been measured from different locations (Mac Arthur and others, 2012). Combined with the noncollimated light source this constructional characteristic of the instrument may affect the comparability of the results of different wavelengths. With eight degree FOV the nominal support was small (3.5 cm) and the difference in the light zenith angle θ_2–θ_1 within the nominal FOV on the sample surface was 0.6° at the highest, whereas the light zenith angle at the bottom of the sample (θ_0) deviated 6.3° from the nominal zenith angle (θ). Mac Arthur and others (2012) found the responsivity of different detectors in ASD to both overlap more and better fill the nominal FOV when smaller support was used. The corresponding backscattering angles reaching the instrument within the FOV varied between 51.3–58.7° and 41.5–43.5° for 8° and 25° FOV, respectively (when direct backscatter is noted by 0°).

Due to the low illumination angle, the possible blockage of irradiance by the snow sampler leading edge was investigated. With eight degree FOV there was no shading of irradiance. In 2013, a 25° FOV was used, potentially increasing the sources of error described above. For these measurements, the deviation in light zenith angles within the instrument FOV is shown in parenthesis in Figure 2b. The light zenith angle at the bottom of the sample (θ_0) deviated 7.8° from the nominal zenith angle, whereas the maximum difference in the light zenith angle within the surface support was 2°. With 25° FOV, the sample holder edge blocked some of the incoming irradiances. However, this mostly affected the response from the sample bottom closer to the light source where the path length of the incoming irradiance within snow is long, leading to an attenuation of the irradiance close to zero. Many studies suggest that most of the responses of snow reflectance are coming from the ~10 cm surface depth (Wiscombe and Warren, 1980; King and Simpson, 2001; Zhou and others, 2003). With the larger FOV the measurement error and uncertainty were increased due to the combination of a noncollimated light source and the biased responsivity of the spectroradiometer. To extend the available dataset, these measurements were retained in the analysis but are marked with an asterisk in the following sections.

Other possible sources of error and uncertainty in the laboratory included anisotropic characteristics of the reference panel and the possible stray light generated by any reflecting surfaces. The accuracy of light zenith angle adjustment was not determined during the experiments. For example, an error of +/− 1 cm in the lamp height would introduce a deviation of +/− 0.26° from the desired zenith angle of 55°.

The consequent radiance acquisitions (10–30) of each snow sample and reference panel allowed the estimation of the integrated precision of the measurements. This was defined by:

$$S(\lambda, \theta) = \frac{1}{N}\sqrt{L_{s1}(\lambda)^2 + L_{s2}(\lambda)^2 + \cdots + L_{sN}^2} \quad (2)$$

where S is the precision, and L_{s1} and L_{s2} are the standard deviations of either the spectralon ($n = 2$–4) or snow ($n = 10$–30) radiance acquisitions at wavelength λ for the individual reference panel and snow samples 1 – N, respectively. Excluding the areas of the low signal-to-noise ratio (SNR) in the beginning and in the end of the spectrum (<400 nm, >2200 nm) and around the detector edges (1000 nm and 1800 nm) the precision error for snow radiance was between $\sim 8.0 \times 10^{-7}$–1.0×10^{-5} W m^{-2} sr^{-1} nm^{-1} and for reference panel radiance between $\sim 2.0 \times 10^{-6}$–8.0×10^{-6} W m^{-2} sr^{-1} nm^{-1}. Any fluctuation in the stability of the instrument or measurement conditions will be integrated into the observed reflectance values. Defining S from the standard deviations of individual snow sample reflectances, defined against the daily averages of 2–4 reference measurements, showed that S varied between 0.0003–0.002 for most of the wavelengths (excluding the areas of low SNR). For the second shortwave infrared (SWIR) detector (1700–2500 nm) S was lower, varying between 0.003–0.004. For snow with a reflectance value of 0.93 these would show a difference of 0.03–0.21% for the first two detectors and 0.32–0.43% for the second SWIR detector.

Separated from the statistical deviations described above are the instrumental uncertainties. The ASD Field Spec utilized in the measurements has undergone absolute radiance and wavelength calibration at the manufacturer on a regular basis. Dark current is a property of the detector, the amount of electronic current due to thermal electrons added to that induced by the incoming photons. Twenty-five dark current measurements were taken, averaged and automatically subtracted from each measured target or reference panel spectrum. The SNR was increased by spectrum averaging. The noise is more apparent where the measured signal strength is low as it was in the range of the second SWIR detector showing the lower precision values above.

Snow always experiences some mechanical and thermodynamic stress when separated from the natural snowpack; slight changes e.g. in snow surface grains may have evolved during the laboratory measurements especially due to the change in ambient temperature. However, this effect was kept small by minimizing the time between

https://doi.org/10.1017/jog.2019.68 Published online by Cambridge University Press

Table 2. Mean and Std dev. of different satellite instrument band specific reflectance values derived from the laboratory measurements

			Snow type							
			D_snow		M_snow		W_snow		W_litter	
Instrument	Band (nm)	Bandwidth (nm)	Mean	Std	Mean	Std	Mean	Std	Mean	Std
VIS										
Terra/Aqua MODIS	Band 3 (459–479)	20	0.97	0.05	0.97 (*−0.0*)	0.07	0.87 (*−9.7*)	0.05	0.78 (*−19.8*)	0.12
Landsat-5 TM	Band 1 (450–520)	70	0.97	0.05	0.97	0.07	0.88	0.05	0.78	0.12
Sentinel-2 MSI	Band 2 (458–523)	65	0.97	0.05	0.97	0.07	0.88	0.05	0.78	0.12
Suomi-NPP VIIRS	Band M3 (478–488)	10	0.97	0.05	0.97	0.07	0.88	0.05	0.78	0.12
Sentinel-3 OLCI	Band 3 (438–448)	10	0.97	0.05	0.97	0.07	0.87	0.06	0.77	0.12
Sentinel-3 OLCI	Band 4 (485–495)	10	0.97	0.05	0.97	0.07	0.88	0.05	0.78	0.12
Landsat-8 OLI	Band 2 (450–510)	60	0.97	0.05	0.97	0.07	0.88	0.05	0.78	0.12
VIS										
Terra/Aqua MODIS	Band 4* (545–565)	20	0.97	0.05	0.97 (*−0.0*)	0.07	0.88 (*−9.2*)	0.05	0.79 (*−18.5*)	0.12
Landsat-5 TM	Band 2 (520–600)	80	0.97	0.05	0.97	0.07	0.88	0.05	0.79	0.12
Sentinel-2 MSI	Band 3 (543–578)	35	0.97	0.05	0.97	0.07	0.88	0.05	0.79	0.12
Sentinel-3 OLCI	Band 6 (555–565)	10	0.97	0.05	0.97	0.07	0.88	0.05	0.79	0.12
Landsat-8 OLI	Band 3 (530–590)	60	0.97	0.05	0.97	0.07	0.88	0.05	0.79	0.12
NOAA AVHRR/3	Band 1 (580-680)	100	0.96	0.05	0.96	0.07	0.87	0.05	0.79	0.11
NIR										
Terra/Aqua MODIS	Band 2 (841–876)	35	0.90	0.06	0.87 (*−2.5*)	0.07	0.73 (*−18.1*)	0.05	0.67 (*−24.8*)	0.11
Landsat-5 TM	Band 4 (760–900)	140	0.90	0.06	**0.89**	0.07	**0.74**	0.05	**0.68**	0.11
Sentinel-2 MSI	Band 8a* (855–875)	20	0.89	0.06	0.86	0.06	0.72	0.05	0.66	0.11
Suomi-NPP VIIRS	Band M7 (846–885)	39	0.89	0.06	0.87	0.06	0.72	0.05	0.66	0.11
Landsat-8 OLI	Band 5 (850–880)	30	0.89	0.06	0.86	0.06	0.72	0.05	0.66	0.11
NOAA AVHRR/3	Band 2 (725-1000)	275	0.88	0.06	**0.84**	0.06	**0.70**	0.06	**0.63**	0.10
SWIR										
Terra/Aqua MODIS	Band 6 (1628–1652)	24	0.12	0.03	0.03 (−76.8)	0.00	0.05 (*−63.8*)	0.04	0.02 (*−87.1*)	0.01
Landsat-5 TM	Band 5 (1550–1750)	200	**0.15**	0.04	0.03	0.00	0.05	0.05	0.02	0.01
Sentinel-2 MSI	Band 11 (1565–1655)	90	0.11	0.03	0.03	0.00	0.04	0.04	0.01	0.01
Landsat-8 OLI	Band 6 (1570–1650)	80	0.11	0.03	0.02	0.00	0.04	0.04	0.01	0.01
NOAA AVHRR/3	Band 3A* (1580-1640)	60	0.11	0.03	0.02	0.00	0.04	0.04	0.01	0.01
NDSI-index (MODIS) (B4-B6)/(B4 + B6)			0.77		0.94		0.90		0.96	

The wavelength range and bandwidth for each band are indicated. For MODIS, relative changes (%) between reflectance of $M_{\_snow}$, $W_{\_snow}$ and $W_{\_litter}$ in relation to $D_{\_snow}$ are shown. The bands are organized with equivalent bands one below another to facilitate the comparison. In the lowermost row, the NDSI indices utilizing the MODIS bands are given.
*Sentinel-3 SLSTR has ~ the same channel.

snow sample extraction and the spectroradiometer measurements. The measured snow types also represent only part of the snow types occurring in nature; notably, very small and very large surface snow grain sizes (e.g. surface hoar) are not present in the dataset. However, the measured snow types and grain sizes represent well the most typical situations in the boreal environment of FMI-ARC as seen from the grain size observations of winters 2011–12 and 2012–13 (Leppänen and others, 2015).

4. Results

Table 1 and Figure 3 summarize the quantitative in situ data available from the measured snow types. Averaged variables describing the snow microstructure for the sampled surface snow (23 cm), determined by the snow pit work at the time of the measurements, are presented in Table 1. The visually estimated typical maximum grain diameters (D_{max}) were weighted by the respective layer depths and the averaged value for the whole snow sample and the surface snow depth of 10 cm were calculated separately. Accordingly, the optical equivalent grain diameter (D_0) is provided if SSA information for the snow type was available. Figure 3 shows the variation of D_0 within the snow samples and the layered snowpack structures with different grain types and sizes. Grain types identified in the snow pit work are presented in Table 4.

According to the snow pit observations, dry snow and wet snow types were characterized by wetness, grain size and density

https://doi.org/10.1017/jog.2019.68 Published online by Cambridge University Press

Table 3. Details of the field dataset used for the characterization of snow reflectance in the SCAmod method (Salminen and others, 2009)

Parameter	Dry snow	Wet snow
Snow depth	54–84 cm	20–73 cm
Snow grain size D_{max}	0.2–2 mm	0.5–3.5 mm
Snow surface wetness (Fierz and others, 2009)	Class 1	Class 2–5
Snow temperature (−5 cm and middle snowpack)	<0 C°	0 C°
No. of measurements	240	450
Measured quantity	BRF	
Illumination	Clear sky/direct	
View angle	Nadir	
Sun zenith angle, θ	50°–75°	
FOV	25°	
Support	20 cm	

differences, the latter having larger (≥1 mm) typical average grain size and higher average density (Table 1). Figure 3 illustrates how the natural snowpack in a boreal environment is both structurally complicated and highly variable in time.

The averaged spectral reflectance (%) for all the measured snow types is presented in Figure 4. The reflectance of dry snow types was close to one in the VIS region. Only $D_{\_crust14}$ deviated from this behavior with slightly lower reflectance in the VIS. More differences between the dry snow types were seen in the NIR region, which is sensitive to the snow grain size and shape. $M_{\_rimed14}$ showed lower reflectance at these longer wavelengths due to moist surface snow. For wet snow types, a distinct drop in reflectance occurred in the NIR region. Surface organic matter in $W_{\_litter13}$ introduced a larger deviation in the observed reflectance values. The amount of organic litter in the snow sample surface within the nominal FOV varied between 0.22–9% two samples being practically free from the litter within this area. The overall Std dev. of reflectance among the different snow types varied between 0.001–0.125 being mostly higher than the precision error of the measurements defined in chapter 3.4.

All the largest differences in the instrument-wise band specific reflectance values within all four snow types (grouped as dry/moist/wet/littered) were detected in NIR bands (Table 2). The maximum difference was 0.05 detected for $M_{\_snow}$ and $W_{\_litter}$ between TM and AVHRR. In the VIS bands, the reflectance values for different band configurations were almost identical with a maximum difference of 0.01. Using MODIS as an example, in the VIS bands, the reflectance of pure and wet snow decreased by ∼10% compared to dry snow whereas the decrease for wet and littered snow was almost 20% (the relative decrease in reflectance (%) for different snow types marked in Table 2). In the NIR bands, the wetness and the consequent grain size growth alone decreased the reflectance by ∼18% compared to dry snow and further decrease by ∼7% were detected due to addition of impurities. The effects of litter and the snow wetness were partially mixed because $W_{\_litter13}$ represented the wettest snow type measured. The largest decrease due to snow wetness and the organic litter was observed in MODIS 6 (1628–1652 nm) and equivalent bands, where $D_{\_snow}$ reflectance was already low but dropped to near zero for the other snow types.

Figure 5 illustrates the MODIS band specific reflectance values and NDSI separately for all ten snow types measured. All snow types showed slightly different band reflectance values. The band specific reflectance or NDSI of wet and littered snow was not unambiguously lower than those of other wet snow types. The NDSI indices for different snow types varied between 0.71–0.97. Finally, in Table 5, the MODIS band specific reflectance values for dry and wet snow types are presented along with those obtained from the field dataset currently utilized in the snow parameterization of the SCAmod method. The values for dry snow are close to each other but differences are more evident for wet snow; for wet snow the laboratory measurements showed lower values by 0.08 and 0.06 for MODIS 3 and MODIS 4, respectively.

5. Discussion

5.1. Spectral reflectance of different snow types

Two distinct groups can be separated based on the averaged spectral reflectance curves presented in Figure 6; dry snow showing high reflectance all over the spectrum and wet snow showing lower reflectance all over the spectrum. Within both groups some differences between the individual snow types could be recognized and in the SWIR range the reflectance of these two groups is partially overlapping. From the deviation in snow reflectance for different snow types in Figure 4 follows that in some occasions wet snow may show higher reflectance than dry snow and vice versa. The total variation in snow reflectance is defined by the maximum and minimum values measured for dry snow and wet snow types, respectively. $M_{\_rimed14}$ with moist surface snow as well as $D_{\_crust14}$ were located in between of these two clear groups. In the following, the factors affecting the different spectral reflectance behavior of the snow types are discussed.

Among the wet snow types, the reflectance of $W_{\_pure13}$ was higher than the reflectance of $W_{\_pure14}$ in the VIS but in the NIR region the difference between the two reversed. The amount of liquid water (Table 1) as well as the visual (D_{max}) and optical equivalent (D_0) grain sizes showed higher values for $W_{\_pure13}$ explaining the reflectance difference. The general consensus is that in wet snow the VNIR (visible-near infrared) spectral surface albedo decreases, not specifically because of the liquid water content, but because of the increase in effective grain size. Liquid water and ice have very similar refractive indices and thus water replacing air between snow grains increases the effective grain size and decreases the surface albedo. In addition, liquid water accelerates the metamorphic grain growth (Wiscombe and Warren, 1980) and promotes the formation of snow grain clusters. This accordingly explains the drop in reflectance for $M_{\_rimed14}$ in the NIR range. Although the difference in the real part of the refractive indices for ice (Warren and Brandt, 2008) and water (Hale and Querry, 1973) is not significant in VNIR and the spectral variation is small (Fig. 7b) the fact that the imaginary part (i.e. the absorption) varies by seven orders of magnitude (Fig. 7c) and that the indices are slightly shifted in wavelength allow, for example, the detection of liquid water content in the snow surface and the identification of the thermodynamic phase of clouds at 1600 nm (Green and others, 2006; Painter and others, 2009; Warren, 2019).

The wet and littered snow showed expectedly the lowest reflectance in the VIS range, otherwise resembling the reflectance curve of $W_{\_pure13}$ measured during the same day. The impurities in snow have most effect at the VIS wavelengths where ice is weakly absorptive (Warren, 1982). However, since the amount of liquid water content was highest for $W_{\_litter13}$ (Table 1) the effects of wetness and litter inclusions were mixed. In Figure 7a the absorption spectra (1 – reflectance) for pine twigs (Niemi and others, 2012) and lichen (spectrometer measurements of snow and bare ground targets and simultaneous measurements of snow conditions/SYKE; FMI) along with spectra for different wet and dry snow types are shown to demonstrate that in the VIS the absorption of the vegetation fragments significantly differs from those of snow. It is expected that the spectral signature of degraded pine needles differs from that of green pine twigs.

https://doi.org/10.1017/jog.2019.68 Published online by Cambridge University Press

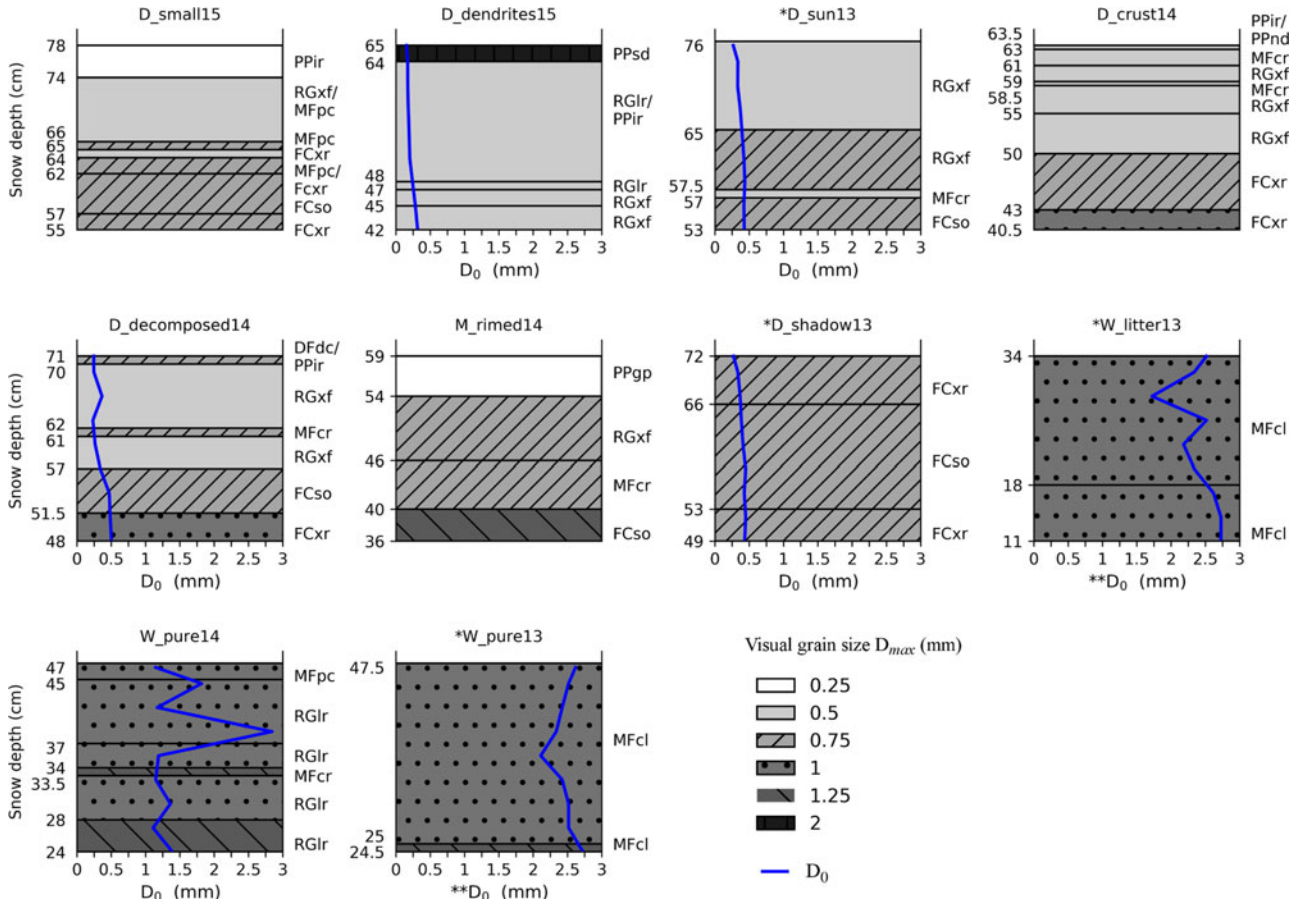

Fig. 3. The snow layers detected in the different snow types based on density, grain size and hardness differences within the snow sample height (23 cm). The snow depth values refer to the actual snow depths of the total snowpack (zero being the ground). For each layer, the snow grain type (Table 4) and the typical grain diameter D_{max} visually estimated to the closest 0.25 mm are presented. Variation of optical equivalent grain diameter (D_0) derived from SSA measurements is identified by the blue line when available. ** is marked for W_litter13 and W_pure13 as the snow wetness may have been in the limit of the SSA instrument measurement capability. Snow types are ordered by increasing D_{max} averaged for the whole snow sample depth (23 cm) (Table 1). Snow types measured with 25 FOV are indicated with *.

Table 4. Classified grain types defined by the snow pit work

PP	Precipitation particles	DF	Decomposing and fragmented precipitation particles	FC	Faceted crystals	RG	Rounded grains	MF	Melt forms
sd	Stellars, dendrites	dc	Partly decomposed	so	Solid faceted	xf	Faceted rounded	cr	Crust
nd	Needles			xr	Rounding facets and corners	lr	Large rounded	cl	Clustered
ir	Irregular							pc	Polycrystals
gp	Graupel, rimed								
sd	Stellars, dendrites								

However, Melloh and others (2001) and Huete (2004) have shown that the absorption remains high until the red edge (680–750 nm) also for bark and nonphotosynthetic litter. Another observation made for $W_{\_litter13}$ was how the organic inclusions had sunk through the snow surface. Peltoniemi and others (2015) deposited high concentrations of soot, silt and volcanic ash on natural snow and noticed that because of the sinking of impurities, the measured BRF darkened at nadir but snow appeared brighter when observed from larger view angles. They continued that an assumption of homogeneous distribution of impurities in models may under- or overestimate the effect of impurities on snow surface albedo. It must be noted that this relationship is dependent on melting conditions, impurity characteristics, view-illumination geometry and whether sufficiently large amounts of organic litter over a large area would exist to have an effect on surface albedo estimates from remote sensing data.

Among the dry snow types, the highest spectral reflectance all over the spectrum was found for $D_{\_denrites15}$ and $D_{\_decomposed14}$ representing new snow. The optical diameter for both, small snow grains and dendrites is small introducing high spectral reflectance. The reflectance of $D_{\_sun13}$ and $D_{\_shadow13}$ dropped after 1000 nm which is in accordance with the larger observed average D_0. $D_{\_crust14}$ showed differing (lower) reflectance behavior from the other dry snow types. A reason may lie in the stratigraphy/microstructure of the snow type; a 0.5 cm thick surface layer of precipitation particles overlie a 2 cm thick melt-freeze crust, followed by a 2 cm of rounded snow grains and another melt-freeze crust. The precipitated snow at the surface probably increased the overall reflectance of this snow type, whereas melt-freeze crusts lowered the amount of scattering. For example, Legagneux and others (2002) measured SSA values for melt-freeze layers which resembled those of rounded grains; before freezing the snow grains have

https://doi.org/10.1017/jog.2019.68 Published online by Cambridge University Press

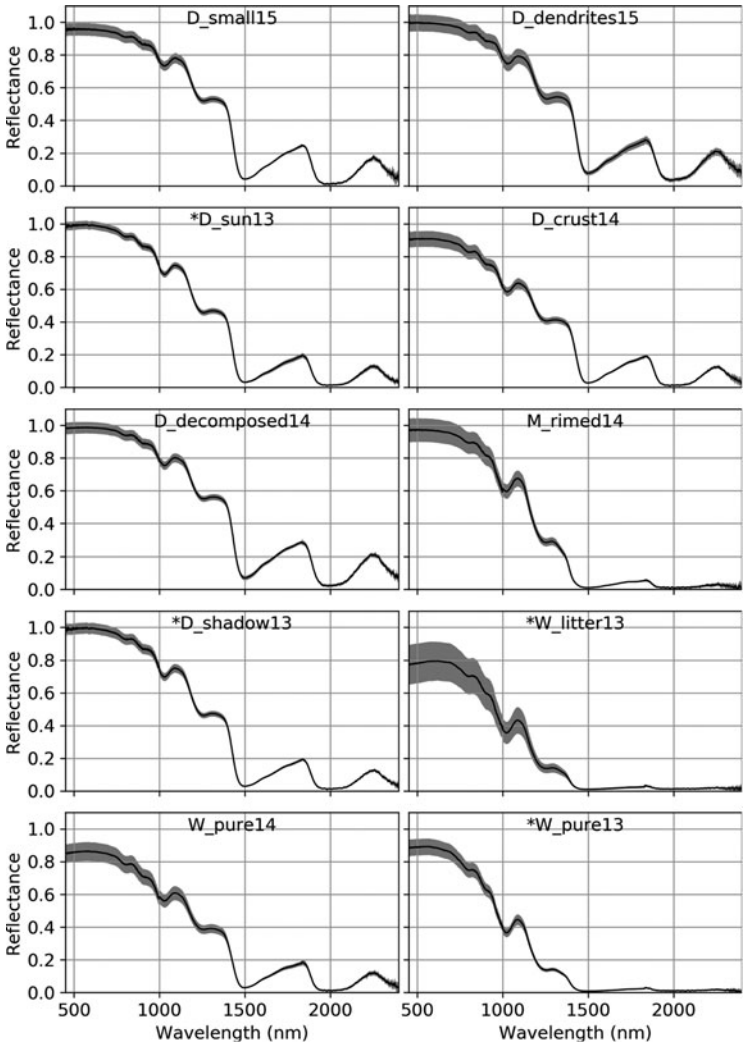

Fig. 4. Average spectral reflectance for different snow types measured with $\theta = 55°$. Shadowed belts show + /− Std dev. determined from snow sample-wise averaged reflectance. Snow types are ordered by increasing (left to right, top to bottom) D_{max} averaged for the whole snow sample depth (23 cm) (Table 1). Snow types measured with 25° FOV are indicated with *.

grown and rounded. The reflectance curve of $D_{\_crust14}$ resembled the curve of $W_{\_pure14}$ despite the rather different stratigraphy observed in the snow pit measurements (Fig. 3).

It is challenging to separate the contribution of snow microstructure on snow spectral reflectance more precisely, as even the critical depth of snow which the measured reflectance is representing may vary between different snow types. The penetration of light in snow is dependent on scattering and absorption mechanisms within the medium (Warren, 1982). These mechanisms vary along wavelength and are affected by impurities, density and snow grain size and grain shape variations. According to Zhou and others (2003) and Wiscombe and Warren (1980), in the VIS range, the 5–20 cm surface snow is the most important for optical remote sensing. Furthermore, Warren (1982) has noted that for the vertical grain size changes to have an effect on snow spectral surface albedo the grain size change must be abrupt and clear, which is the case, for example, when a thin layer of newly precipitated snow overlies a deep layer of old snow. In our experiments, a rather thin layer of precipitated surface snow seemed to dominate over the deep underlying layer of more metamorphosed snow (e.g. 1 cm in $D_{\_decomposed14}$).

Especially in the NIR range, also the grain shape affects the spectral reflectance (Xie and others, 2006). In their numerical study, Picard and others (2009) showed that spheres reflected 20–30% less than other grain shapes for the same SSA. Snowpacks with very similar average snow grain sizes but differing snow stratifications (varying snow layers and grain sizes) can yield very different spectral surface albedos (Zhou and others, 2003). For broadband surface albedo, taking into account the vertical variation in snow grain size produces satisfactory results as this averaged quantity is not very sensitive to details of the angular distribution of scattering. Directional quantities including spectral reflectance (here approximating BRF) are more sensitive to the effects of the snow grain shape which affects the scattering phase function (Jin and others, 2008). Snow reflectance anisotropy has been observed to increase along increasing wavelength, grain size and solar zenith angle and depends on the grain shape as well (Carroll and Fitch, 1981; Warren, 1982; Steffen, 1987). Although these laboratory experiments measured at nadir do not offer information on the reflectance angular distribution, it is noted that differing scattering phase functions for different snow grain shapes may explain some of the differences observed in the reflectance behavior of the snow types measured. For example, comparisons by Xie and others (2006) of five different ice crystal habits showed that BRF for all shapes decreased along with increasing effective grain size in the NIR region but at different rates; BRF for aggregates decreased slowest whereas the reflectance of plates showed the highest variations.

The importance of snow density on snow reflectance is emphasized by its effect on the optical depth. Light penetrates deeper into snow with low density and/or large snow grain size than snow with high density and/or small snow grain size; the vertical variation in snow density affects the critical snow depth the measured reflectance is representing (Zhou and others, 2003). Low density offers more air/ice interfaces for light scattering and increases the path length of a photon at wavelengths

https://doi.org/10.1017/jog.2019.68 Published online by Cambridge University Press

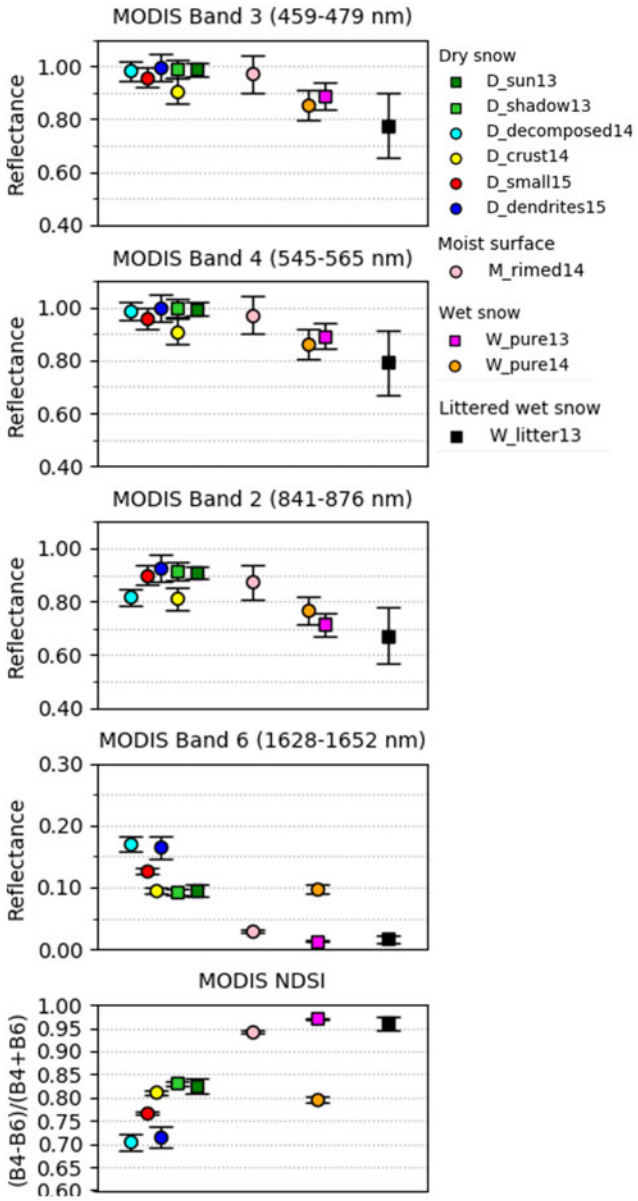

Fig. 5. MODIS band specific reflectance values and NDSI for all the different snow types resampled from the laboratory measurements. The whiskers show + /− Std dev.. Measurements conducted with 25° FOV are shown by rectangle shapes.

where scattering is dominant. On the other hand, longer path length enhances the probability for a photon to become absorbed. The measured reflectance per wavelength is thus defined by a complex relationship of the ability of each snow layer to absorb, scatter and penetrate the light into snow (King and Simpson, 2001).

5.2. Band specific reflectance of different satellite sensors

Despite the various band configurations of the different satellite sensors they produced almost equal results in the VIS range. However, more dispersion was observed in the NIR and SWIR range, refer to Table 2. For example, the relative maximum difference in reflectance in NIR bands was 2.2, 5.6, 5.4 and 7.4% for $D_{\_snow}$, $M_{\_snow}$, $W_{\_snow}$ and $W_{\_litter}$, respectively. In the SWIR range the band specific reflectance of TM and AVHRR for $D_{\_snow}$ differed 26.7%. An increase of differences from the visible towards the longer wavelengths is in accordance with the fact that the reflectance is more sensitive to snow characteristics, such as grain size and liquid water content on the NIR and SWIR regions.

The largest deviations from the average values seem to be produced by the widest bands such as AVHRR band 2 (275 nm) or TM band 5 (200 nm) whereas the maximum differences between the narrower bands was 0.01. In addition to different band configurations, the varying spectral response functions affect the reflectance values. Trishchenko and others (2002) found that for similar surface spectral reflectance and atmospheric conditions, for example, MODIS 1 and 2 showed a difference of up to 30–40% in reflectance and NDVI relative to AVHRR due to different satellite sensor SRFs. The information that there is not necessarily any particular change in snow reflectance for close-by bands is relevant for the use of different historic or present satellite sensors (e.g. AVHRR, Sentinel-2 and −3) for the mapping of snow cover, especially concerning the production of long climate data records with multiple instruments.

The best bands to detect the difference between dry and wet snow proved to be the bands located in the NIR range where the most pronounced decrease in reflectance was seen due to snow wetness and the consequent snow grain size growth. The changes in the SWIR bands produced high relative differences due to low reflectance values. Higher NDSI indices for moist and wet snow types than for dry snow were obtained (Table 2, last row) being in accordance with findings of Negi and others (2010) and Niemi and others (2012), who observed that NDSI increased along snow aging and increasing snow moisture content.

Since SSA has been observed to be linked to SWIR reflectance (Picard and others, 2009) it has been suggested if the SWIR wavelengths (e.g. MODIS 6) observed from space could offer a method to follow the evolution of snow microphysical characteristics (Domine and others, 2006). For example, Salzano and others (2016) kept the reaction of SWIR reflectance on precipitation events, and as such, on snow type changes, in their experimental data from Ny-Ålesund, Svalbard, as a promising observation. In these laboratory experiments, the difference between newly precipitated snow (e.g. $D_{\_dendrites15}$) and wet snow (e.g. $W_{\_pure13}$) was clear, but for example, dry snow $D_{\_sun13}$ and wet snow $W_{\_pure14}$ introduced quite similar results to each other (Fig. 5). In MODIS 2 the Std dev. e.g. between $W_{\_pure14}$, $D_{\_crust14}$ and $D_{\_decomposed14}$ was overlapping; the wet snow reflectance was not always lower than the reflectance of dry snow, nor was reflectance of wet littered snow always lower than that of pure wet snow. The latter was affected by the high variability in the amount of litter inclusions. However, it is noted that for the averaged values, obtained for the snow types grouped either as dry or wet, the difference between the band reflectance values was clear. As indicated by Table 2, the discussion about the MODIS band reflectance values of different snow types is also valid for other sensors.

5.3. Improvement of snow reflectance parameterization for snow mapping algorithms

The field spectroscopy-based MODIS band specific reflectance values were close to those retrieved from the laboratory experiments (Table 5). The differences were more evident for wet snow. The effect of the illumination angle on the observed reflectance values is widely recognized and usually taken into account when in situ data of snow reflectance are used as a model input parameter or as validation/calibration data for the model output in SCA mapping (e.g. Painter and others, 2009). However, the SCAmod method characterizes dry and wet snow (end-member) reflectance simply as a static average and Std dev. of the observations collected under various snow and illumination conditions. The inaccuracy in the pre-determined reflectance values propagates in the uncertainty of snow cover maps. The wet snow

https://doi.org/10.1017/jog.2019.68 Published online by Cambridge University Press

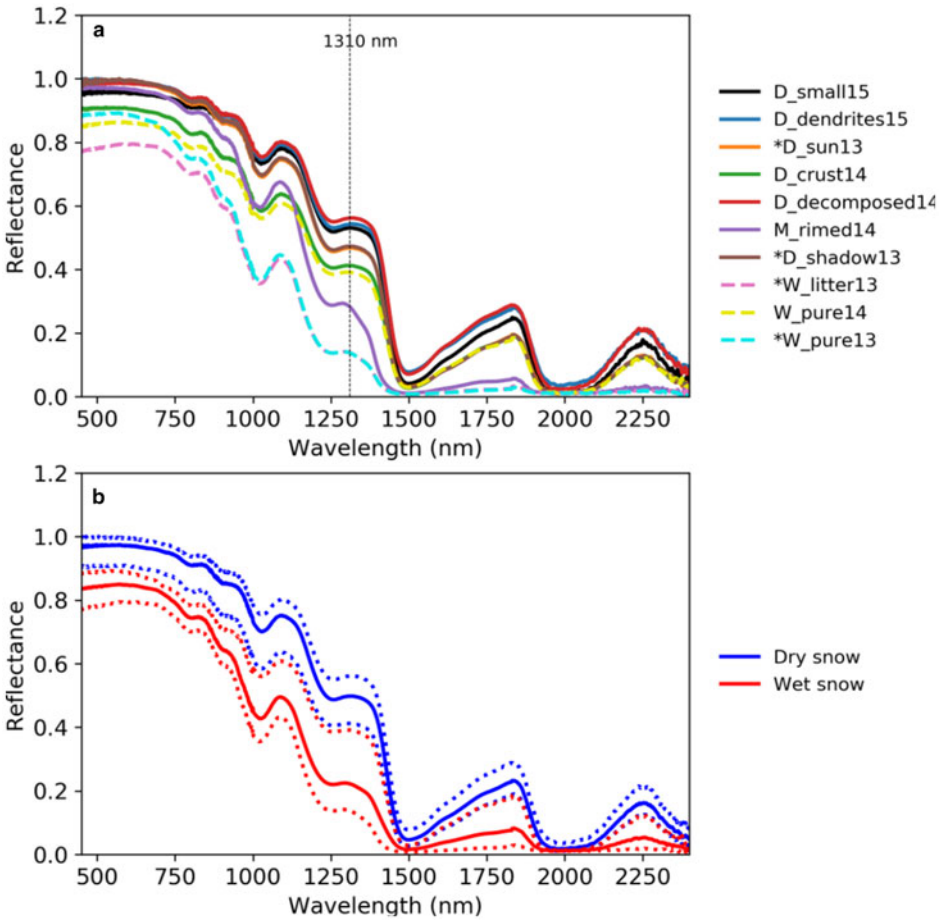

Fig. 6. (a) Average spectral reflectance of all the snow types measured. The wavelength used for SSA measurements is indicated with a dotted line. Snow types measured with 25° FOV are indicated with *. In (b) the average, minimum and maximum for two explicit snow type groups, wet and dry snow, defined by their spectral behavior are presented.

Table 5. Field measurement results for MODIS band specific reflectance by Salminen and others (2009) in direct illumination

MODIS	Band 3 (459–479 nm)				Band 4 (545–565 nm)				Band 6 (1628–1652 nm)			
	Mean Field	*Lab*	Std Field	*Lab*	Mean Field	*Lab*	Std Field	*Lab*	Mean Field	*Lab*	Std Field	*Lab*
Dry snow	1.00	*0.97*	0.08	*0.05*	0.98	*0.97*	0.10	*0.05*	0.09	*0.12*	0.06	*0.03*
Wet snow	0.95	*0.87*	0.09	*0.05*	0.94	*0.88*	0.10	*0.05*	0.03	*0.05*	0.01	*0.04*

The corresponding values from laboratory experiments are shown in *italics.*

reflectance obtained from the field data for MODIS 3 and 4 was comparatively high, taking into account that the measurements observed with higher light zenith angles should lower the mean value (e.g. Painter and others, 2004). The results suggest that the field spectroscopy-based values (Salminen and others, 2009) for dry snow reflectance characterization are quite good but values used for wet snow reflectance in remote sensing data retrieval algorithms may be too high (Metsämäki and others, 2015).

6. Conclusions

In this study, we assessed the reflectance variability of natural snowpacks based on measurements of snow samples under controlled illumination conditions. The laboratory measurement setup facilitated the retrieval of the effect of snow characteristics and organic impurities on snow reflectance without the disturbance by changing illumination evident in field spectroscopy. The results of this study can be directly used to refine accuracy characterization and parametrization of snow mapping algorithms utilizing reflectance information of spectral end-members, such as snow. Better characterization of the true variability of snow reflectance will decrease the uncertainty of the snow cover maps produced by optical remote sensing.

The results indicated that most of the snow types could be grouped either as dry or wet based on their spectral behavior. However, some snow types were located between these two distinct groups, such as snow with the moist surface and snow with the near-surface melt-freeze crusts. The relationship between varying snow sample microstructures and snow spectral reflectance proved to be challenging. It was hypothesized that this was due to differing critical surface snow depths contributing to the measured spectral reflectance, and combined effects of the snow grain size and shape differences between the several snow surface layers. From the snow characteristics, only snow grain size increase connected to the snow wetness and the addition of organic litter inclusions systematically changed the observed spectral reflectance.

The resampling of the laboratory measurements to correspond to various satellite instrument bands indicated that despite the various band configurations the results were similar for most of the bands with a maximum difference of 0.01. More deviation was seen in the NIR and SWIR bands which are more sensitive to the snow grain size and liquid water content. Largest deviations

https://doi.org/10.1017/jog.2019.68 Published online by Cambridge University Press

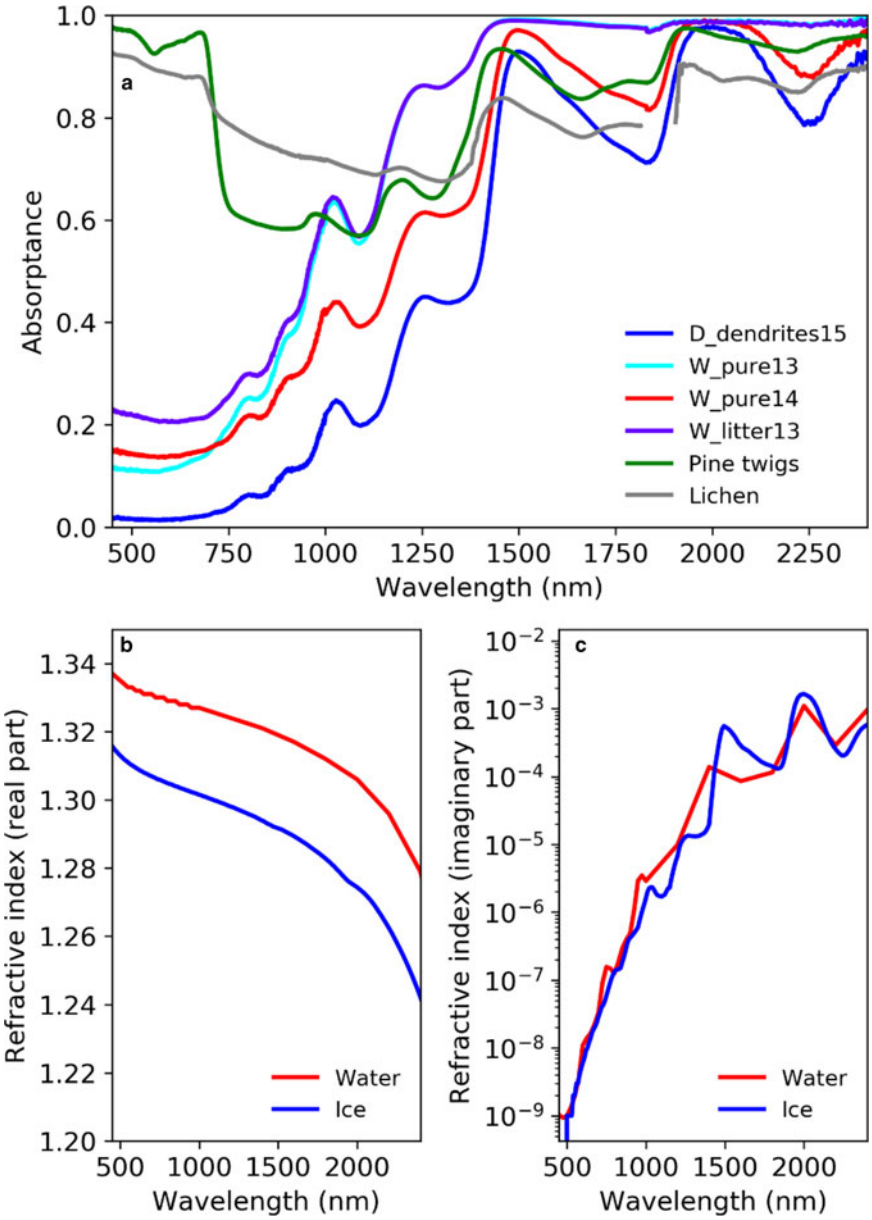

Fig. 7. (a) An example of the absorptance spectra (1 – reflectance) for pine twigs and lichen as well as for $D_{\_dendrites15}$ and the different wet snow types. The wavelengths at the water absorption band ~1900 nm were removed for lichen spectra due to the low SNR. In (b) real part and in (c) imaginary part of the refractive index for ice and water are presented.

in the band reflectance values were produced by the widest band configurations. The laboratory results were compared by means of MODIS band specific reflectance values with field spectroscopy observations currently used to describe the snow reflectance variability in the snow cover mapping method SCAmod. The results suggested that the values used for wet snow reflectance in remote sensing data retrieval algorithms may need refinement, e.g. field spectroscopy results (Salminen and others, 2009) reported slightly higher values than those obtained here for channels relevant to snow detection (Metsämäki and others, 2015). These results are also valid for other sensors as the observed effect of different band configurations and SRF on snow reflectance were indicated to be small.

Acknowledgements. This research was funded by Maj and Tor Nessling foundation. It has also been supported by the A4-project (Arctic Absorbing Aerosols and Albedo of Snow, decision No. 254195), Nordic Top-level Research Initiative (TRI) 'Cryosphere-atmosphere interactions in a changing Arctic climate' (CRAICC), funded by the Academy of Finland.

Author contribution. HRH was responsible for the planning, coordination and execution of the laboratory experiments. She analyzed the data and wrote most of the paper. JP was behind the measurement idea, took part in the writing work and acted as the scientific supervisor.

References

Aoki T and 5 others (2000) Effects of snow physical parameters on spectral albedo and bidirectional reflectance of snow surface. *Journal of Geophysical Research* **105**(D8), 10219–10236. doi: 10.1029/1999JD901122.

Brown RD and Robinson DA (2011) Northern hemisphere spring snow cover variability and change over 1922–2010 including an assessment of uncertainty. *Cryosphere* **5**, 219–229. doi: 10.5194/tc-5-219-2011.

Bruegge CJ, Martonchik JV and Stahler AH (2000) A review of reflectance nomenclature used in remote sensing. *Journal of Geophysical Research* **19**, 9–20.

Carroll JJ and Fitch BW (1981) Effects of solar elevation and cloudiness on snow albedo at the south pole. *Journal of Geophysical Research* **86**(C6), 5271–5276. doi: 10.1029/JC086iC06p05271.

Claverie M and 7 others (2018) The harmonized landsat and sentinel-2 surface reflectance data set. *Remote Sensing of Environment* **219**, 145–161. doi: 10.1016/j.rse.2018.09.002.

Dietz AJ, Kuenzer C, Gessner U and Dech S (2012) Remote sensing of snow – a review of available methods. *International Journal of Remote Sensing* **33** (13), 4094–4134. doi: 10.1080/01431161.2011.640964.

Domine D and 5 others (2006) Correlation between the specific surface area and the short wave infrared (SWIR) reflectance of snow. *Cold Regions Science and Technology* **46**(1), 60–68. doi: 10.1016/j.coldregions.2006.06.002.

Dozier J, Green RO, Nolin AW and Painter TH (2009) Interpretation of snow properties from imaging spectrometry. *Remote Sensing of Environment* **113**, S25–S27. doi: 10.1016/j.rse.2007.07.029.

Dumont M, Brissaud O, Picard G, Gallet JC and Arnaud Y (2010) High-accuracy measurements of snow bidirectional reflectance distribution function at visible and NIR wavelengths – comparison with modelling results. *Atmospheric Chemistry and Physics* **10**, 2507–2520. doi: 10.5194/acp-10-2507-2010.

Fierz C and 8 others (2009) The International Classification for Seasonal Snow on the Ground. *IHP-VII Tech. Doc. Hydrol.* N83, IACS Contribution N1, UNESCO-IHP, Paris.

Gallet J-C, Domine F, Zender CS and Picard G (2009) Measurement of the specific surface area of snow using infrared reflectance in an integrating sphere at 1310 and 1550 nm. *Cryosphere* **3**, 167–182. doi: 10.5194/tc-3-167-2009.

Green RO, Dozier J, Roberts D and Painter T (2002) Spectral snow-reflectance models for grain-size and liquid-water fraction in melting snow for the solar-reflected spectrum. *Annals of Glaciology* **34**, 71–73. doi: 10.3189/172756402781817987.

Green RO, Painter T, Roberts DA and Dozier J (2006) Measuring the expressed abundance of the three phases of water with an imaging spectrometer over melting snow. *Water Resources Research* **42**(W10402). doi: 10.1029/2005WR004509.

Groisman PY, Karl TR and Knight RW (1994) Observed impact of snow cover on the heat balance and the rise of continental spring temperatures. *Science* **263**, 198–200. doi: 10.1126/science.263.5144.198.

Hadley OL and Kirchstetter TW (2012) Black-carbon reduction of snow albedo. *Nature Climate Change* **2**, 437–440. doi: 10.1038/NCLIMATE1433.

Hale GM and Querry MR (1973) Optical constants of water in the 200-nm to 200-μm wavelength region. *Applied Optics* **12**(3), 555–563.

Hall DK, Foster JL and Chang ATC (1992) Reflectance of snow as measured in situ and from space in sub-Arctic areas in Canada and Alaska. *IEEE Transactions on Geoscience and Remote Sensing* **30**(3), 634–637. doi: 10.1109/36.142947.

Huete AR (2004) Remote sensing for environmental monitoring. In Artiola JF Pepper IL and Brusseau ML (ed.), *Environmental Monitoring and Characterization*. Burlington, USA: Elsevier Academic Press, pp. 183–206.

Jin Z, Charlock TP, Yang P, Xiw Y and Miller W (2008) Snow optical properties for different particle shapes with application to snow grain size retrieval and MODIS/CERES radiance comparison over Antarctica. *Remote Sensing of Environment* **112**, 3563–3581. doi: 10.1016/j.rse.2008.04.011.

Kaasalainen S and 5 others (2006) Optical properties of snow in backscatter. *Journal of Glaciology* **52**(179), 574–584. doi: 10.3189/172756506781828421.

King MD and Simpson WR (2001) Extinction of UV radiation in Arctic snow at alert, Canada (82°N). *Journal of Geophysical Research* **106**(D12), 12499–12507. doi: 10.1029/2001JD900006.

Kokhanovsky AA and Zege EP (2004) Scattering optics of snow. *Applied Optics* **43**(7), 1589–1602.

Kokhanovsky AA, Aoki T, Hachikubo A, Hori M and Zege EP (2005) Reflective properties of natural snow: approximate asymptonic theory versus in situ measurements. *IEEE Transactions on Geoscience and Remote Sensing* **43**(7), 1529–1535.

Legagneux L, Cabanes A and Dominé F (2002) Measurement of the specific surface area of 176 snow samples using methane adsorption at 77K. *Journal of Geophysical Research* **107**(D17). doi: 10.1029/2001JD001016.

Leppänen L, Kontu A, Vehviläinen J, Lemmetyinen J and Pulliainen J (2015) Comparison of traditional and optical grain size field measurements with SNOWPACK simulations in a taiga environment. *Journal of Glaciology* **61**(225), 151–162. doi: 10.3189/2015JoG14J026.

Lv Y and Sun Z (2014) The reflectance and negative polarization of light scattered from snow surfaces with different grain size in backward direction. *Journal of Quantitative Spectroscopy & Radiative Transfer* **133**, 472–481. doi: 10.1016/j.jqsrt.2013.09.010.

Mac Arthur A, MacLellan CJ and Malthus T (2012) The fields of view and directional response functions of two field spectroradiometers. *IEEE Transactions on Geoscience and Remote Sensing* **50**(10), 3892–3907. doi: 10.1109/TGRS.2012.2185055.

Melloh RA, Hardy JP, Davis RE and Robinson PB (2001) Spectral albedo/reflectance of littered forest snow during the melt season. *Hydrological Processes* **15**(18), 3409–3422. doi: 10.1002/hyp.1043.

Metsämäki SJ, Anttila ST, Huttunen JM and Vepsäläinen JM (2005) A feasible method for fractional snow cover mapping in boreal zone based on a reflectance model. *Remote Sensing of Environment* **95**, 77–95. doi: 10.1016/j.rse.2004.11.013.

Metsämäki SJ and 5 others (2012) An optical reflectance model-based method for fractional snow cover mapping applicable to continental scale. *Remote Sensing of Environment* **123**, 508–521. doi: 10.1016/j.rse.2012.04.010.

Metsämäki SJ and 8 others (2015) Introduction to GlobSnow snow extent products with considerations for accuracy assessment. *Remote Sensing of Environment* **156**, 96–108. doi: 10.1016/j.rse.2014.09.018.

Nakamura T, Abe O, Hasegawa T, Tamura R and Ohta T (2001) Spectral reflectance of snow with a known grain-size distribution in successive metamorphism. *Cold Regions Science and Technology* **32**(1), 13–26. doi: 10.1016/S0165-232X(01)00019-2.

Negi HS, Singh SK, Kulkarni AV and Semwal BS (2010) Field-based spectral reflectance measurements of seasonal snow cover in the Indian Himalaya. *International Journal of Remote Sensing* **31**(9), 2393–2417. doi: 10.1080/01431160903002417.

Nicodemus FE, Richmond JC, Hsia JJ, Ginsberg IW and Limperis T (1977) *Geometrical Considerations and nomenclature for Reflectance*. Washington: National Bureau of Standards, US Department of Commerce.

Niemi K and 6 others (2012) The behaviour of mast-borne spectra in a snow-covered boreal forest. *Remote Sensing of Environment* **124**, 551–563. doi: 10.1016/j.rse.2012.06.008.

Painter TH and Dozier J (2004) Measurements of the hemispherical-directional reflectance of snow at fine spectral and angular resolution. *Journal of Geophysical Research* **109**(D18), D18115, 1–21. doi: 10.1029/2003JD004458.

Painter TH, Dozier J, Roberts DA, Davis RE and Green RO (2003) Retrieval of subpixel snow-covered area and grain size from imaging spectrometer data. *Remote Sensing of Environment* **85**, 64–77. doi: 10.1016/S0034-4257(02)00187-6.

Painter TH and 5 others (2009) Retrieval of subpixel snow covered area, grain size and albedo from MODIS. *Remote Sensing of Environment* **113**, 868–879. doi: 10.1016/j.rse.2009.01.001.

Peltoniemi JI, Kaasalainen S, Näränen J, Matikainen L and Piironen J (2005) Measurement of directional and spectral signatures of light reflectance by snow. *IEEE Transactions on Geoscience and Remote Sensing* **43**(10). doi: 10.1109/TGRS.2005.855131.

Peltoniemi JI and 12 others (2015) Soot on snow experiment: bidirectional reflectance factor measurements of contaminated snow. *Cryosphere* **9**(6), 2323–2337. doi: 10.5194/tc-9-2323-2015.

Picard G, Arnaud L, Domine F and Fily M (2009) Determining snow specific surface area from near-infrared reflectance measurements: numerical study of the influence of grain shape. *Cold Regions Science and Technology* **56**(1), 10–17. doi: 10.1016/j.coldregions.2008.10.001.

Pulliainen J, Salminen M, Heinilä K, Cohen J and Hannula H-R (2014) Semi-empirical modeling of the scene reflectance of snow-covered boreal forest: validation with airborne spectrometer and lidar observations. *Remote Sensing of Environment* **155**, 303–311. doi: 10.1016/j.rse.2014.09.004.

Pulliainen J and 19 others (2017) Early snowmelt significantly enhances boreal springtime carbon uptake. *Proceedings of the National Academy of Sciences* **114**(42), 11081–11086. doi: 10.1073/pnas.1707889114.

Salminen M, Pulliainen J, Metsämäki S, Kontu A and Suokanerva H (2009) The behavior of snow and snow-free reflectance in boreal forests: implications to the performance of snow covered area monitoring. *Remote Sensing of Environment* **113**(5), 907–918. doi: 10.1016/j.rse.2008.12.008.

Salminen M and 5 others (2018) Determination of uncertainty characteristics for the satellite data-based estimation of fractional snow cover. *Remote Sensing of Environment* **212**, 103–113. doi: 10.1016/j.rse.2018.04.038.

Salzano R, Lanconelli C, Salvatori R, Esposito G and Vitale V (2016) Continuous monitoring of spectral albedo of snowed surfaces in Ny-Ålesund. *Rendiconti Lincei. Scienze Fisiche e Naturali* **27**, 137–146.

Sandmeier S, Müller C, Hosgood B and Andreoli G (1998) Sensitivity analysis and quality assessment of laboratory BRDF data. *Remote Sensing of Environment* **64**(2), 176–191. doi: 10.1016/S0034-4257(97)00178-8.

Schaepman-Strub G, Schaepman ME, Painter TH, Dangel S and Martonchik JV (2006) Reflectance quantities in optical remote sensing – definitions and case studies. *Remote Sensing of Environment* **103**(1), 27–42. doi: 10.1016/j.rse.2006.03.002.

https://doi.org/10.1017/jog.2019.68 Published online by Cambridge University Press

Sihvola A and Tiuri M (1986) Snow fork for field determination of the density and wetness profiles of a snow pack. *IEEE Transactions on Geoscience and Remote Sensing* **GE-24**(5), 717–721.

Steffen K (1987) Bidirectional reflectance of snow at 500–600 nm. In *Large scale effects of seasonal snow cover (Proceedings of the Vancouver Symposium), August, 1987*, IAHS Publ., 166, Wallingford, UK, pp. 415–425.

Trishchenko AP, Cihlar J and Li Z (2002) Effects of spectral response function on surface reflectance and NDVI measured with moderate resolution satellite sensors. *Remote Sensing of Environment* **81**(1), 1–18. doi: 10.1016/S0034-4257(01)00328-5.

Vaughan DG and 13 others (2013) Observations: cryosphere. In Stocker TF and 9 others (eds), *Climate Change 2013: The Physical Science Basis. Contribution of Working Group I to the Fifth Assessment Report of the Intergovernmental Panel on Climate Change*. Cambridge: Cambridge University Press, pp. 317–382.

Vikhamar D and Solberg R (2002) Subpixel mapping of snow cover in forests by optical remote sensing. *Remote Sensing of Environment* **84**, 69–82. doi: 10.1016/S0034-4257(02)00098-6.

Vikhamar D and Solberg R (2003) Snow-cover mapping in forests by contrained linear spectral unmixing of MODIS data. *Remote Sensing of Environment* **88**, 309–323. doi: 10.1016/j.rse.2003.06.004.

Warren SG (1982) Optical properties of snow. *Reviews of Geophysics and Space Physics* **20**, 67–89.

Warren SG (1984) Impurities in snow: effects on albedo and snowmelt. *Annals of Glaciology* **5**, 177–179.

Warren SG (2019) Optical properties of ice and snow. *Philosophical Transactions of the Royal Society A* **377**. doi: 10.1098/rsta.2018.0161.

Warren SG and Brandt RE (2008) Optical constants of ice from the ultraviolet to the microwave: a revised compilation. *Journal of Geophysical Research* **113**(D14220). doi: 10.1029/2007JD009744.

Winther J-G (1993) Short- and long-term variability of snow albedo. *Nordic Hydrology* **24**(2–3), 199–212.

Winther J-G and 5 others (1999) Spectral reflectance of melting snow in a high Arctic watershed on Svalbard: some implications for optical satellite remote sensing studies. *Hydrological Processes* **13**(12–13), 2033–2049.

Wiscombe WJ and Warren SG (1980) A model for the spectral albedo of snow. I. Pure snow. *Journal of the Atmospheric Sciences* **37**, 2712–2733.

Xie Y, Yang P, Gao B-C, Kattawar GW and Mishchenko MI (2006) Effect of ice crystal shape and effective size on snow bidirectional reflectance. *Journal of Quantitative Spectroscopy and Radiative Transfer* **100**, 457–469. doi: 10.1016/j.jqsrt.2005.11.056.

Zender CS, Dominé F, Gallet J-C and Picard G (2009) Darkening of soot-doped natural snow: measurements and model. In Pedersen CA, Bernsten TK, Gerland S and Warren SG (eds), *Report From the International Workshop: Black Carbon in Snow – Sampling, Albedo Effects and Climate Impact, 13 August-14 August 2009, Tromsø, Norway, Vol. 017*, Tromsø: Norwegian Polar Institute, pp. 40–44.

Zhou X, Li S and Stamnes K (2003) Effects of vertical inhomogeneity on snow spectral albedo and its implication for optical remote sensing of snow. *Journal of Geophysical Research* **108**(D23), 4738. doi: 10.1029/2003JD003859.

https://doi.org/10.1017/jog.2019.68 Published online by Cambridge University Press